CeO_2 Nanocatalysts

DOI: 10.1002/ange.201108849

First-Principles Design of Highly Active and Selective Catalysts for Phosgene-Free Synthesis of Aromatic Polyurethanes**

*Siris Laursen, Diego Combita, Ana B. Hungría, Mercedes Boronat, and Avelino Corma**

In memory of Purificación Escribano

The substitution of phosgene by safer and more environmentally friendly reactants in the synthesis of aromatic polyurethanes is still an unsolved issue. An industrial reaction of considerable interest for producing isocyanates, which are precursors of aromatic polyurethanes,[1,2] is the *N*,*N*′-dicarbamoylation of diaminotoluene (DAT) by dimethylcarbonate (DMC), a "green" reagent which can be produced from CO_2 and methanol.[3] The selective reaction proceeds by the transfer of two methoxycarbonyl ($-COOCH_3$) groups from DMC to DAT to produce the desired dicarbamoylated product **3**. In the unselective process DAT is methylated instead, producing **4** and **5** along with polymethylated and mixed methylated and carbamoylated products **6** (Scheme 1).

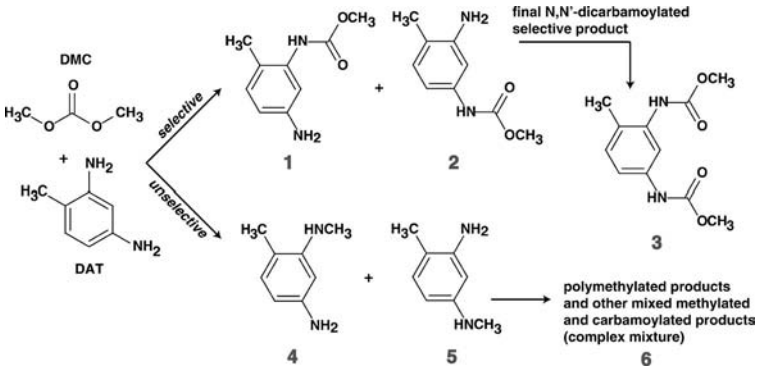

Scheme 1. Reaction of dimethylcarbonate (DMC) with diaminotoluene (DAT).

We have recently presented a gold catalyst that allows the production of dicarbamates from dialkylcarbonates and diamino compounds under mild reaction conditions.[4] It was shown that gold supported on CeO_2 nanoparticles is more selective than gold supported on TiO_2, Fe_2O_3, or on larger CeO_2 particles. It was also observed that gold-free CeO_2 nanoparticles (ca. 5 nm) were already quite selective. This result suggests that it is possible to avoid the use of gold, provided that highly active and selective catalysts could be prepared from pure CeO_2.

Herein, we show that quantum chemical calculations combined with the synthesis of nanocrystallites of CeO_2 with well-defined crystal sizes and shapes can be used to design solid catalysts that allow for the production of carbamates from aromatic amines and DMC with good selectivity, circumventing the use of hazardous phosgene.[5–7]

As a first step, the molecular reaction mechanism of aniline carbamoylation over the three most thermodynamically stable stoichiometric CeO_2 surfaces, the {111}, {110}, and {100} facets, was investigated by means of density functional theory calculations. The reaction pathway for DMC dissociation starts with the adsorption of DMC in the less stable *trans* configuration, with the carbonyl oxygen interacting with a Ce^{4+} site (Scheme 2). The calculated adsorption energies, −0.19, −0.48, and −0.50 eV on the {111}, {110}, and {100} facets, respectively, match well with the coordination of the Ce^{4+} adsorption site. The {111} surface presents Ce^{4+} sites with seven surrounding oxygens, and the {110} and {100} surfaces present Ce^{4+} sites with six surrounding oxygens.

The selective DMC dissociation proceeds through a transition state in which the oxygen atoms of the CeO_2 surface (O_{surf}) play a key role in activating DMC (Supporting Information, Figure S1). Formation of a new $C-O_{surf}$ bond leads to a structure with a tetrahedral CO_4 geometry similar to that found in the transition states for SN2 reaction mechanisms, which facilitates the scission of the $CH_3OCO-OCH_3$ bond. The calculated activation barriers for this step are similar over all three crystal surfaces and are less than 0.4 eV (Figure 1 and Table 1), indicating that the dissociation of DMC to yield the desired $-COOCH_3$ fragment should readily occur at low temperatures on the three surfaces studied.

Two different unselective DMC decomposition pathways were next investigated. The direct $-CH_3$ transfer from adsorbed DMC to the oxide surface according to path 1

[*] Dr. S. Laursen, D. Combita, Dr. M. Boronat, Prof. A. Corma
Instituto de Tecnología Química, Universidad Politécnica de Valencia—Consejo Superior de Investigaciones Científicas
Av. Naranjos s/n, 46022 Valencia (Spain)
E-mail: acorma@itq.upv.es
Dr. A. B. Hungría
Departamento de Ciencia de los Materiales e Ingeniería Metalúrgica y Química Inorgánica, Facultad Ciencias, Universidad de Cádiz
Campus Rio San Pedro, 11510 Puerto Real, Cádiz (Spain)

[**] We thank the Generalitat Valenciana (GV/2009/063 and PROMETEO 2088/130) and the Spanish MICINN (MAT2011-28009, and Consolider Ingenio 2010-MULTICAT: CSD2009-00050) for financial support. We thank *Red Española de Supercomputación* (RES) for computational resources. D.C. thanks Spanish MICINN for a post-graduate scholarship, and S.L. thanks ITQ for a post-doctoral fellowship.

Supporting information for this article (including the Experimental Section and optimized geometries of all structures investigated) is available on the WWW under http://dx.doi.org/10.1002/anie.201108849.

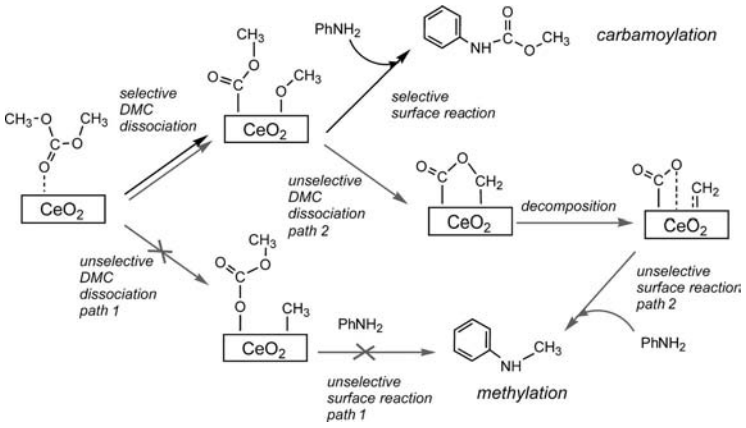

Scheme 2. Proposed mechanism for carbamoylation and methylation of $PhNH_2$ over CeO_2. Black arrows show the preferred pathway for {111} and {110} surfaces. Dark gray arrows show the preferred pathway for the {100} surface.

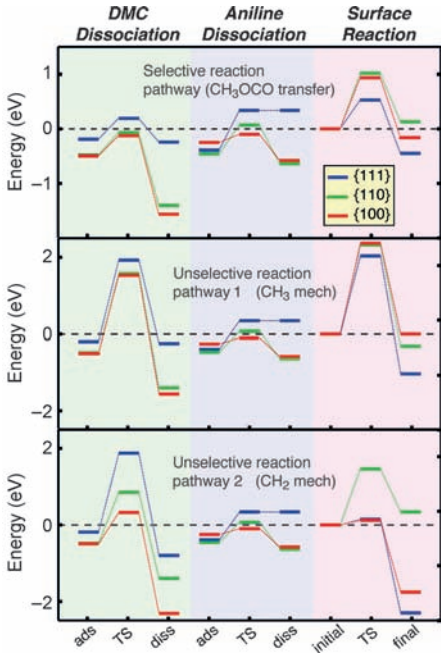

Figure 1. Energetics of selective (carbamoylation) and unselective (methylation) reaction pathways in the reaction of DMC and aniline over the stoichiometric {111}, {110}, and {100} surfaces of CeO_2.

Table 1: Calculated activation barriers (in eV) for the key elementary steps depicted in Scheme 2.

Elementary step	{111}	{110}	{100}
Selective DMC dissociation	0.34	0.37	0.37
Unselective DMC dissociation: path 1	2.17	2.45	2.03
Unselective DMC dissociation: path 2	2.06	1.34	0.82
Aniline deprotonation	0.73	0.53	0.07
Selective surface reaction	0.53	0.78	0.94
Unselective surface reaction: path 1	2.04	2.32	2.37
Unselective surface reaction: path 2	0.15	1.47	0.12

(Scheme 2 and Figure 1) involves activation barriers larger than 2.0 eV on all three CeO_2 surfaces, suggesting that this mechanism is not likely to occur. The high activation barriers are caused by the lack of interaction between the transferring $-CH_3$ group and the CeO_2 surfaces in the corresponding transition states (Supporting Information, Figure S2). According to path 2 (Scheme 2 and Figure 1) the $-OCOCH_3$ fragment formed in the selective dissociation of DMC deprotonates and subsequently decomposes into $-CH_2-$ and CO_2. Here the basicity of the surface O_{surf} atoms plays a direct role in promoting the deprotonation step, and the calculated barriers decrease almost linearly from 2.06 eV on the {111} surface to 0.82 eV on the {100} surface (Table 1). This trend suggests that this undesired deprotonation step will barely occur on the {111} facet, but might be fast on the {100} facet. After deprotonation, the remaining $-COO-CH_2-$ fragment is strongly bound to the CeO_2 surface through two $C-O_{surf}$ bonds, indicating that this fragment, if produced, would be thermodynamically trapped and could easily decompose into CO_2 and a $-CH_2-$ group. Indeed, this decomposition step was calculated on the {100} surface, where the probability of having the $-COO-CH_2-$ fragment is larger, and it was found to be approximately barrierless.

The second reactant, aniline, adsorbs on all CeO_2 surfaces, interacting with a Ce^{4+} site through the nitrogen atom (Supporting Information, Figure S4). The calculated adsorption energies of aniline are −0.39, −0.46, and −0.25 eV on the {111}, {110}, and {100} facets, respectively. Deprotonation occurs by direct transfer of one hydrogen atom to an oxygen atom of the surface, and the basicity of the O_{surf} atom again determines the activation barrier for this step (Table 1). Once deprotonated, the $PhNH-$ fragment remains attached to one Ce^{4+} site. The selective surface reaction between deprotonated aniline and a $-COOCH_3$ fragment on the {111} and {110} surfaces occurs through a transition state similar to that found for the selective dissociation of DMC, in which the C atom bonded to an O_{surf} atom has a nearly tetrahedral coordination (Supporting Information, Figure S5). Since the thermodynamic stability of the fragments involved in the selective coupling is considerably larger on the {110} and {100} facets than on the lower energy {111} surface (Figure 1), higher activation barriers are also obtained for the former two facets. The calculated activation energy for the selective coupling step is 0.94 eV on the {100} facet and 0.78 eV on the {110} facet. In both cases this becomes the rate-determining step of the reaction. On the {111} surface, however, the barrier for the surface reaction is only 0.53 eV. Thus, on the {111} surface the rate-determining step is the deprotonation of aniline, which has a barrier of 0.73 eV. This indicates that, while all unselective dissociation pathways on the {111} surface involve barriers larger than 2 eV, the activation energies calculated for the elementary steps in the selective reaction are lower than 0.53 eV. Taking this into account, it can already be concluded that the {111} surface of CeO_2 should be highly selective for carbamoylation. A similar conclusion can be arrived at for the {110} surface, although with a smaller difference between the activation barriers for the selective

coupling step (0.78 eV) and the unselective dissociation (1.34 eV).

The calculated activation energies for the unselective reaction between deprotonated aniline and a surface methyl group are larger than 2.0 eV on all surfaces, again due to the fact that the transfer of the methyl group is not stabilized by any interaction with the CeO_2 surface (Supporting Information, Figure S6). This pathway can therefore be ruled out on all CeO_2 surfaces. The alternative unselective pathway involving a $-CH_2-$ group transfer to PhNH– was found to be almost barrierless over the {111} and {100} surfaces indicating that, if unselective DMC dissociation occurs, formation of unselective methylated products is unhindered at any reaction temperature. However, according to Scheme 2 and the calculated barriers summarized in Table 1, $-CH_2-$ groups are only formed on the {100} facet, suggesting that this CeO_2 surface will probably lead to formation of undesired methylated products.

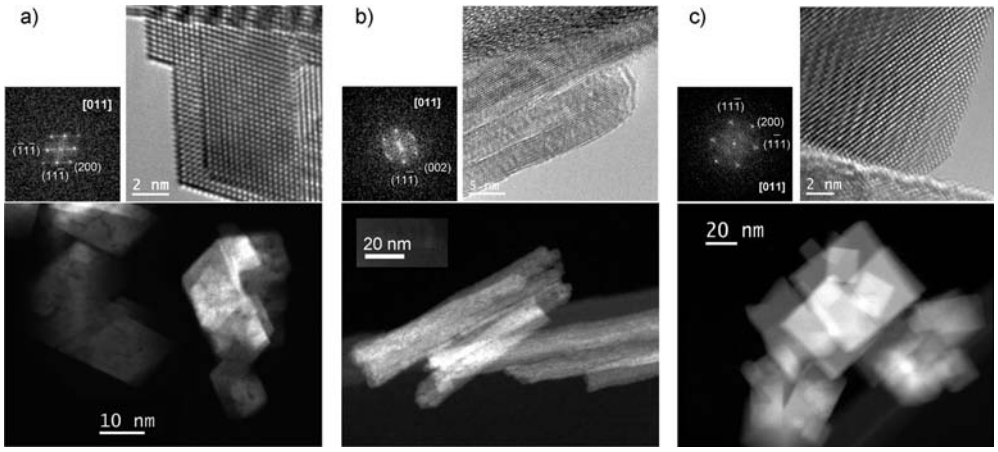

Figure 2. TEM images of the three CeO_2 nanostructures: a) Octahedra, b) Rods, and c) Cubes.

Finally, to close the catalytic cycle, the pathway for the desorption of $-OCH_3$ surface fragments was calculated. These fragments leave as methanol, which is formed by reaction of the $-OCH_3$ groups with adsorbed hydrogen atoms generated during aniline deprotonation. It was found that the formation of methanol takes place without an activation barrier over all CeO_2 surfaces. This means that this step is not kinetically limiting and that there is no threat of $-OCH_3$ and H atoms poisoning the catalyst surface by remaining strongly adsorbed.

The activity of partially reduced surface sites towards DMC dissociation was also investigated (Supporting Information, Figure S7) and it was found that oxygen vacancies are indeed highly active sites for binding and dissociating DMC. However, once dissociated, the fragments of DMC (CH_3OCOO-, CH_3O-, or CO_3) readily heal the oxygen vacancy through their terminal oxygens, releasing significant energy. Regeneration of the active sites through CH_3OH formation and desorption is prohibitively endothermic, indicating that oxygen vacancy defects, even if present at the beginning of the reaction, will be immediately healed without the possibility of being regenerated, and the reaction will proceed over the stoichiometric CeO_2 surface thereafter.

On the basis of the theoretical study, a selective CeO_2 catalyst for carbamoylation of aromatic amines should preferentially expose stoichiometric {111} or {110} facets and avoid {100} facets. Following this, three well-defined structure-directed CeO_2 nanocrystals preferentially exposing {111}, {110}, and {100} facets, respectively, were synthesized and their catalytic performance in the carbamoylation of DAT was tested. The three CeO_2 nanostructures were produced by a hydrothermal method in H_2O, using $Ce(NO_3)_3$ as the metal source and NaOH to produce seeds and direct to the particular structure.[8] By varying the concentration of NaOH and the temperature of the hydrothermal treatment, nano-octahedra, nanorods, or nanocubes terminated by {111}, {110}, and {100} surface facets, respectively, were obtained (Figure 2). The synthetic method and the specific conditions of NaOH concentration and temperature are described in detail in the Supporting Information.

The catalytic performance of the three nanocrystals in the carbamoylation of DAT by DMC is shown in Figure 3. The catalytic tests were performed as batch reactions in thick-walled glass reactors of approximately 50 mL volume. After the reactor was charged with reactants and catalyst, the headspace was purged and then backfilled with argon to a pressure of 3 bar. A temperature of 140 °C was employed for all reactions. Octahedra and rods performed similarly in the reaction, producing over 90 % conversion in the first 30 min, with yields of monocarbamoylated DAT close to 80 %. The

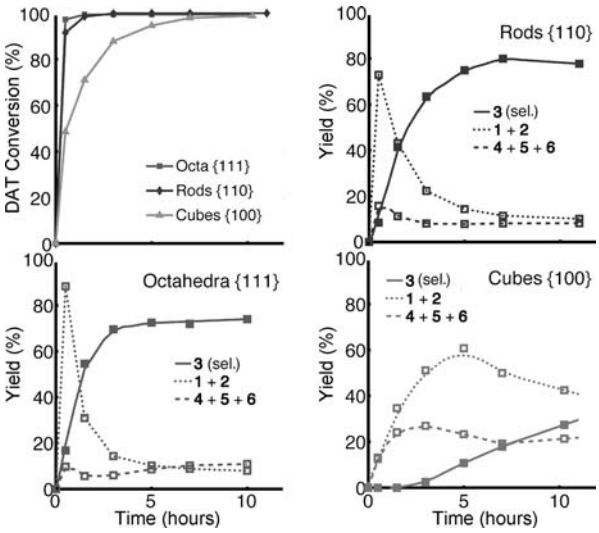

Figure 3. Carbamoylation of DAT over CeO_2 nanostructures. Conversion and yield of dicarbamoylated DAT (——), monocarbamoylated DAT (••••) and methylated products (– – –) obtained using nano-octahedra, nanorods, and nanocubes of CeO_2 as catalyst.

monocarbamoylated species are then rapidly converted into the desired dicarbamoylated DAT, with final selectivities of 80% and 85% on octahedra and rods, respectively. The cubes had a much slower reaction rate and a lower selectivity for dicarbamoylated DAT (ca. 25% at 10 h), which is in line with the predictions of the theoretical study. From the calculated activation energies for selective DMC dissociation ($E_a <$ 0.4 eV) and previous spectroscopic studies, it is known that DMC dissociates selectively over all three surfaces at relatively low temperature, which likely results in CeO_2 surfaces covered with $-COOCH_3$ and $-OCH_3$ fragments. In this situation, the selectivity is determined by the difference between the barrier for the selective surface coupling reaction and that for the unselective decomposition of the $-COOCH_3$ fragments. As previously described, this difference is at a maximum on the {111} facet.

As for the unselective process, the methylation of DAT occurs only at the start of the reaction over the octahedra and rods. However, the production of methylated products over the cubes is as fast as the production of monocarbamoylated DAT, and continues throughout the entire reaction. Again, this observation agrees with the theoretical results, which showed that formation of unselective methylated products requires the presence of surface $-CH_2-$ species, and that this species is mainly produced by decomposition of the selectively dissociated DMC fragment $-COOCH_3$ over the {100} facet. Furthermore, the barriers calculated for the surface reaction between $-CH_2-$ and PhNH$-$ (see Table 1) indicate that, if both species are present, they will readily react to form the methylated product. Altogether, it becomes clear that the unselective dissociation of DMC to form $-CH_2-$ surface species controls the formation of methylated products and the overall selectivity, and that low energy facets like {111} can be used to circumvent this reaction from occurring.

In summary, first-principles calculations show that the selectivity of CeO_2 catalysts toward carbamoylation can be rationally tuned by changing the crystal shape. All stoichiometric CeO_2 surfaces are able to dissociate DMC selectively with low barriers, but low energy facets have inherently lower activity towards the unselective decomposition of DMC and additionally promote the selective surface coupling reaction between $-COOCH_3$ and $-NHPh$ by weakly binding these intermediate species. The catalytic performance of the three synthesized structure-directed CeO_2 nanocrystals preferentially exposing {111}, {110}, and {100} facets, respectively, confirms the predictions of the theoretical study. An optimum catalyst consisting of CeO_2 nano-octahedra preferentially exposing the {111} facets has been developed and shown to be both highly active and selective for DAT dicarbamoylation without the use of phosgene.

Received: December 15, 2011
Revised: February 6, 2012
Published online: March 21, 2012

Keywords: carbamoylation · crystal shape · density functional calculations · green chemistry · nanocrystals

[1] K. Weissermel, H. J. Harpe in *Industrial Organic Chemistry*, 4th ed., Wiley-VCH, Weinheim, **2003**.
[2] *Kirk-Othmer Encyclopedia of Chemical Technology*, 4th ed., Wiley, New York, **1994**.
[3] Y. Ono, *Appl. Catal. A* **1997**, *155*, 133–166.
[4] R. Juárez, P. Concepción, A. Corma, V. Fornés, H. Garcia, *Angew. Chem.* **2010**, *122*, 1308–1312; *Angew. Chem. Int. Ed.* **2010**, *49*, 1286–1290.
[5] I. Lee, F. Delbecq, R. Morales, M. A. Albiter, F. Zaera, *Nat. Mater.* **2009**, *8*, 132–138.
[6] M. B. Boucher, S. Goergen, N. Yi, M. Flytzani-Stephanopoulos, *Phys. Chem. Chem. Phys.* **2011**, *13*, 2517–2527.
[7] B. N. Zope, D. D. Hibbitts, M. Neurock, R. J. Davis, *Science* **2010**, *330*, 74–78.
[8] H. Mai, L. Sun, Y. Zhang, R. Si, W. Feng, H. Zhang, H. Liu, C. Yan, *J. Phys. Chem. B* **2005**, *109*, 24380–24385.

